AIP | Physics of Fluids

Undulatory microswimming near solid boundaries

R. D. Schulman, M. Backholm, W. S. Ryu, and K. Dalnoki-Veress

Citation: Physics of Fluids (1994-present) **26**, 101902 (2014); doi: 10.1063/1.4897651
View online: http://dx.doi.org/10.1063/1.4897651
View Table of Contents: http://scitation.aip.org/content/aip/journal/pof2/26/10?ver=pdfcov
Published by the AIP Publishing

PHYSICS OF FLUIDS **26**, 101902 (2014)

Undulatory microswimming near solid boundaries

R. D. Schulman,[1] M. Backholm,[1] W. S. Ryu,[2] and K. Dalnoki-Veress[1,3,a)]
[1]*Department of Physics and Astronomy and the Brockhouse Institute for Materials Research, McMaster University, Hamilton, Ontario L8S 4M1, Canada*
[2]*Department of Physics and the Donnelly Centre, University of Toronto, Toronto, Ontario M5S 1A7, Canada*
[3]*Laboratoire de Physico-Chimie Théorique, UMR CNRS Gulliver 7083, ESPCI, Paris, France*

(Received 23 June 2014; accepted 26 September 2014; published online 16 October 2014)

The hydrodynamic forces involved in the undulatory microswimming of the model organism *C. elegans* are studied in proximity to solid boundaries. Using a micropipette deflection technique, we attain direct and time-resolved force measurements of the viscous forces acting on the worm near a single planar boundary as well as confined between two planar boundaries. We observe a monotonic increase in the lateral and propulsive forces with increasing proximity to the solid interface. We determine normal and tangential drag coefficients for the worm, and find these to increase with confinement. The measured drag coefficients are compared to existing theoretical models. The ratio of normal to tangential drag coefficients is found to assume a constant value of $1.5 \pm 0.1(5)$ at all distances from a single boundary, but increases significantly as the worm is confined between two boundaries. In response to the increased drag due to confinement, we observe a gait modulation of the nematode, which is primarily characterized by a decrease in the swimming amplitude.
 [http://dx.doi.org/10.1063/1.4897651]

I. INTRODUCTION

Locomotion through a fluid environment at small length scales, or "microswimming," is interesting because the relevant physics differs considerably from that applicable to macroscopic swimmers. Microorganisms dwell in a regime where viscous forces dominate and swimmers have negligible inertia.[1] That is, the Reynolds number (Re), which is a measure quantifying the ratio of inertial to viscous forces in a fluid, is typically much smaller than unity for microscopic swimmers. The activity within this field has increased substantially in recent years. This growth is, in part, due to rapidly improving experimental techniques capable of performing measurements of motile microorganisms, as well as more developed analytical and computational treatments of these systems. Beyond studies which have succeeded in providing precise kinematic observations of small swimmers, in the last decade, there have been direct force measurements of unicellular organisms using optical traps.[2,3] This large drive towards developing a better understanding of low Re locomotion is warranted, as it offers exciting application and research avenues, such as fluid pumping,[4–6] collective motion of bacteria to generate mixing in microfluidic devices,[7,8] and microscopic artificial swimmers capable of transporting loads for biomedical purposes such as advanced drug targeting and robotic surgery.[9,10] Furthermore, enhancing our ability to describe the relevant physics is a crucial step towards developing a more complete picture of the behaviours, capabilities, and interactions of bacteria, sperm, and other microorganisms.

There are numerous biologically relevant systems in which microorganisms move near a boundary, such as in surface-associated bacterial infections,[11,12] sperm locomotion in the female reproductive tract,[13] and biofilm formation.[14,15] To attain a complete picture of these systems, it is imperative to understand how the physics of a microswimmer differs upon proximity to an interface. However,

a)Electronic mail: dalnoki@mcmaster.ca

microswimmers are typically studied while swimming in an effectively infinite fluid and few studies have investigated the effects of a nearby interface. In particular, due to the nearby no-slip boundary condition at a fluid-solid interface, there will be an increase in the shear of the velocity field near such a boundary. This increase in shear will cause an increase in viscous forces, which will influence the motility of organisms. Experiments have verified changes in both propulsion and trajectories of swimmers near solid boundaries at low Re.[6,16–18]

A unique aspect of low Re locomotion is that, according to the Scallop Theorem, to achieve propulsion it is necessary to undergo a sequence of motions that is not time-reversible.[1] Microorganisms have developed various swimming mechanisms that satisfy this constraint, such as motions akin to a human breast stroke, as characterized by the alga cell *Chlamydomonas reinhardtii*,[19,20] or the helical rotation of a bacterium's flagellum.[1,21,22] Undulatory locomotion, in which a swimmer propagates travelling waves down the length of its body, is another non-time-reversible mechanism, and is often employed by nematodes and sperm.[23–26]

Undulatory locomotion has proved to be a highly efficient means of propulsion which is present over length scales ranging from micrometers to tens of meters.[27] The locomotion of slender undulatory swimmers has been investigated by a multitude of theoretical studies.[22,25,26,28,29] A common approach is to derive resistance coefficients for the swimmer, such that given the velocity of the segments of the swimmer's body, it is possible to compute the force. Such a framework is called resistive force theory (RFT). In this model, one can decompose the force acting on each body segment into a component tangential and normal to the body, each of which is proportional to the speed of the segment along the corresponding direction, and related by the normal and tangential drag coefficients, c_N and c_T. In particular, the ratio $K = c_N/c_T$ is a quantity of interest, as it determines the magnitude and direction of propulsion of the swimmer. These drag coefficients have been derived for a slender undulator in an unbounded fluid[22,25] and for slender cylinders near boundaries.[30,31] In particular, the results of Katz *et al.* predict $K = 2$ for a cylinder moving parallel to a nearby fluid-solid interface, and also predict K to increase past a value of 2 when the cylinder is confined between parallel solid plates.[30] Recently, the drag coefficients of an undulatory microswimmer in an infinite fluid were found using direct force measurements, and compared well with the theoretical result.[32] However, there have been no direct force or drag coefficient measurements for undulatory swimmers in proximity to a solid boundary, which is the focus of this study.

Experiments focusing on undulatory locomotion often employ the model organism *Caenorhabditis elegans*,[33] a millimeter sized nematode, as its subject. The viscoelastic material properties of this worm have been determined,[34] as well as its kinematic properties in a wide variety of media.[35–43] In addition, there has been much interest in the gait modulation of *C. elegans* from swimming to crawling, which involves a decrease in frequency and wavelength of undulatory motion.[35–37] The gait modulation is known to occur in response to changing environmental resistance, which has been realized in experiments by changing viscosity,[35,36] and by pressing the worm down onto an agar surface with a glass plate.[44] Direct force measurements have been attained for *C. elegans* crawling on agar[45,46] and recently for *C. elegans* swimming in a buffer.[32] Although there have been some studies which have involved confining the worm,[44,47] no experiments have measured swimming forces in proximity to an interface, nor have the kinematics been studied for confinement of the worm near solid boundaries. Despite this, many studies of free swimming *C. elegans* employ experimental designs in which the worm swims near a solid boundary, even though the effects of the boundary, in terms of changing drag coefficients and modulations in kinematics of the worm, are not properly understood. Studying the behaviour and forces experienced by *C. elegans* in confinement provides insight into the impact of the physical constraints that nematodes face in their true habitats (e.g., soils and other materials with small interstitial spaces).

In this paper, we perform direct force measurements using micropipette deflection[32,34,48,49] on the undulatory microswimmer and model organism *C. elegans* at controlled distances from a singe solid boundary and between two solid boundaries. The structure of the paper is as follows. In Sec. II, we describe the experimental methods, including details of micropipette deflection and image analysis. In Sec. III A, we present measurements of forces and drag coefficients of the worm at varying distances from a single planar solid boundary, and compare these to existing theoretical models. In Sec. III B, we determine drag coefficients for the worm swimming midway between two

planar solid boundaries with different spacings, and compare the measurements to theory. We discuss and present evidence of a gait modulation of the worm in response to increasing drag coefficients in confinement in Sec. III C. Finally, we provide a summary and conclusions in Sec. IV. We find that for increasing confinement, the drag coefficients and viscous forces generated by *C. elegans* increase monotonically. The drag coefficients are compared to theoretical models and exhibit partial agreement. We determine the drag coefficient ratio K, and find that it is constant at all distances from the single boundary, but find it to increase as the worm is confined between two boundaries. In addition, as the drag coefficients increase, the worm is seen to exhibit a gait modulation.

II. EXPERIMENTAL METHODS

A. Micropipette deflection

As in previous work, we employ a micropipette deflection technique to measure time-resolved forces in dynamic, microscale systems.[32,34,48,49] In this experimental technique, a flexible glass micropipette that is more than three orders of magnitude thinner than it is long, deflects when subjected to an external force. The pipette can be calibrated by ejecting a small droplet through the pipette which then hangs off the pipette tip. By imaging the droplet, and calculating its volume, the mass of the droplet can be found. Observing the deflection of the pipette in response to the droplet's weight allows the spring constant to be determined. Once the spring constant is known, a pipette can be used as a force transducer, for which the deflections away from the equilibrium position indicate the applied force. For instance, the pipette can be pushed against a soft material to measure its properties.[34,49] Since the pipette is hollow, suction can be applied to catch objects at the end of the pipette. Using this set up, one can perform friction and adhesion measurements,[48] or measure the forces generated by an active object.[32]

In this study, two types of pipettes are employed. In the first part of the study, a straight pipette with an L-shaped bend at its end is used (Fig. 1(a)). The L-shaped bend, in which each length is about 300–600 μm, is highly rigid compared to the long straight portion of the pipette, which is roughly 3 cm long. For this reason, only the long straight portion exhibits appreciable deflection. Therefore, this micropipette is capable of deflecting in two perpendicular directions: along the worm's swimming axis, as well as along the corresponding in-plane perpendicular direction (Fig. 1(b)). Thus, using this pipette, we can measure both the propulsive and lateral hydrodynamic forces generated by the worm, by simply observing the L-shaped bend from below (the same approach has previously been employed[32]). In the second part of the study, a completely straight pipette which is roughly 3 cm long is used (Fig. 1(c)). Such a pipette can only deflect side-to-side, and can thus only measure

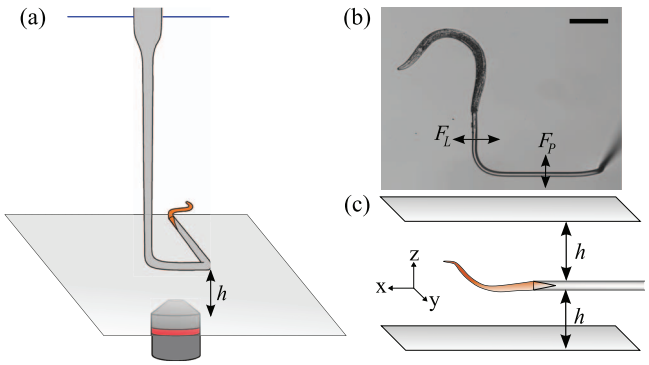

FIG. 1. (a) Experimental set up for the single boundary experiments. A straight pipette with an L-shaped bend at its end is used to measure forces of the worm swimming at a distance h from the boundary. The blue horizontal line represents the location of the buffer meniscus. (b) An image taken of a young adult worm swimming as it is being held with the L-shaped bend of a pipette. By observing the L-shaped bend move, we can measure both lateral (F_L) and propulsive (F_P) forces. The scalebar represents 200 μm. (c) Experimental set up for the channel confinement experiments. A straight pipette is used to measure lateral forces of the worm swimming in the x-y plane at a distance h from each boundary.

the lateral forces generated by the worm. All pipettes in this study have an outer diameter of $\sim$20 μm and an inner diameter of $\sim$10 μm. The spring constants of all pipettes are within the range of 2.7–8.9 nN/μm, with no more than 10% uncertainty in each spring constant. The deflections of the pipettes in these experiments are much smaller than length scales associated with swimming of the worms. Thus, pipettes can be treated as linear springs, and drag forces acting on the pipette are small compared to the forces driving it.

B. Experimental design

In this study, force measurements are performed on worms in the so called L4, young adult, and adult life stages. For the purpose of our study, these are different sized worms that behave in the same way when captured. Wild-type worms (N2) were obtained from the Caenorhabditis Genetics Center and cultivated according to standard procedures.[33] The worms are picked off NGM plates and placed inside a chamber filled with M9 for the force measurements (see Fig. 1). Worms are captured by positioning the end of the micropipette in proximity to the worm's tail and applying suction through a syringe connected to the micropipette. Worms are never sucked in by more than 15% of their total length. Upon capture, the z-position of the pipette is adjusted and monitored using a digital actuator. The nematodes perform a highly reproducible undulatory motion when being held by the micropipettes. Since the worm is being constrained in its motions, we expect the propulsive forces generated by a tethered worm to be smaller than a freely swimming worm. Worms are seen to swim in the plane of focus (parallel to the plane of the boundaries) during the majority of the experiments, as they are captured while swimming parallel to this plane. In each type of experiment, the system is observed from below with a microscope. Images of the swimming are taken with a high-speed camera (Allied Vision Technologies, Model: GT1660) at 56 fps. Data in which there are out of plane swimming results in the worm's body being out of focus during a portion of the swimming cycle – such data are discarded.

Worms are studied in two types of confinement: near a single planar boundary and inside a channel. For the single planar boundary experiment, a transparent cylindrical container is used.[32] In this case, the micropipette with the L-shaped bend is inserted into the chamber from above such that the thin flexible portion is fully immersed in the fluid, as seen in Fig. 1(a), where the horizontal line indicates the location of the buffer meniscus. By letting the thick stiff portion of the pipette pass through the meniscus, we prevent capillary forces at the contact line from disturbing the force measurements. The L-shaped bend is in a plane parallel to the bottom boundary. For the measurements, the worm is positioned to be at a desirable h away from the bottom boundary. The distance h is measured by moving the pipette until it is in contact with the bottom surface, and subsequently raising the pipette while keeping track of the relative change in height using the digital actuator.

For the channel confinement experiment, the channel is composed of two parallel glass slides spaced and held together by a chosen number of layers of melted Parafilm to achieve a desired channel height, $2h$ (Fig. 1(c)). The channel heights range from 58 μm to 1700 μm. This channel is mounted within a larger chamber filled with buffer in which the worms are placed, composed of two horizontal glass slides separated by rubber spacers. The buffer remains in the chamber due to surface tension. In these experiments, the straight pipette is inserted into the larger chamber from the side. For the measurements, the worm is captured from the larger chamber and positioned such that it is equidistant from the top and bottom plates of the internal channel, at a distance h from either plate. The flexible portion of the pipette is mainly in the larger chamber, and only a small portion at the end (containing the worm) is placed within the channel in order to reduce the drag force on the pipette. Again, we ensure that the meniscus of the buffer is only in contact with the thicker portion of the pipette. The height of the channel $2h$ and the corresponding midpoint position are determined using the same technique as for the single boundary.

C. Image analysis

The deflections of the micropipettes are analyzed using a cross-correlation technique, which, given the magnification of the microscope used in the experiment, is able to resolve deflections to

a precision of ∼0.1 μm. This translates into a sub nN precision in our force measurements for the range of pipette spring constants used.

The nematode's motion during swimming is analyzed as follows. First, each snapshot of the swimming is thresholded into a binary image. Subsequently, each binary image is processed to attain a centerline of the worm's body. The raw data of each centerline are smoothed using a spline curve. From the resultant smoothed centerline, which is composed of 1000 equally spaced points, it is possible to compute quantities such as body curvatures and the amplitude of the swimming. The velocity of a body point in a given frame (used for the RFT computations) is calculated by measuring the difference in position of the point in the previous frame to that in the next frame. This procedure leads to a ∼5% error in computing the velocities. All above analysis was done using inhouse code written in MATLAB. The worm's radius is measured near its vulva using ImageJ.

III. RESULTS AND DISCUSSION

A. Single planar boundary

1. Force measurements

At any distance from the boundary, lateral and propulsive force curves over a swimming cycle of the worm were obtained. The force curves were reproducible over time as well as from worm to worm. Examples of force curves for a single period of swimming at a distance close and far from the boundary are shown in Figs. 2(a) and 2(b). The Reynold's number of this system is in the range

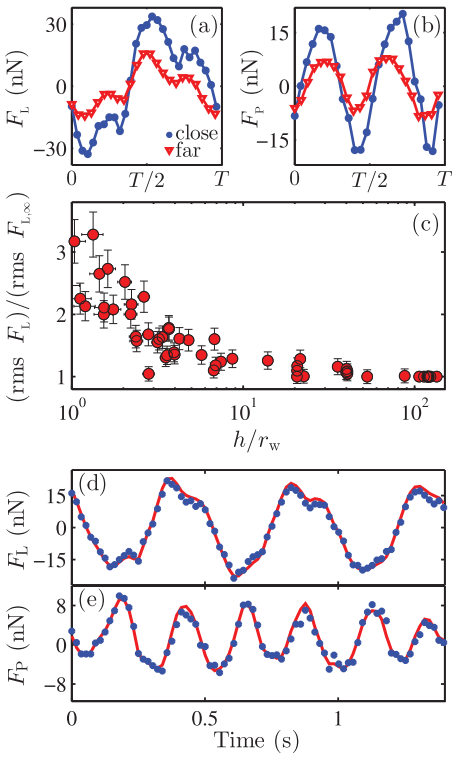

FIG. 2. The (a) lateral (F_L) and (b) propulsive (F_P) forces over one period of a young adult worm's swimming, close ($h = 35 \pm 4$ μm) and far ($h = 2524 \pm 4$ μm) from a single boundary. (c) The rms lateral force normalized to its value at infinity ($h/r_w > 100$) as a function of the distance to the boundary (h) normalized by the worm radius (r_w), for young adult worms. The vertical error bars come from uncertainties in the spring constant of the pipette and temporal variations of the forces. The horizontal error bars stem from uncertainties in determining the distance from the boundary and measuring the worm's radius. The vertical error bars increase for larger forces, since the percentage error for all data points is similar. (d) Lateral and (e) propulsive forces (blue circle markers) for a young adult worm swimming near a single boundary ($h/r_w \sim 2.8$) plotted as a function of time over several periods. The solid red curves correspond to simultaneous RFT fits to the lateral and propulsive force data. In this case, $c_N = 7.8 \pm 1.2$ and $c_T = 5.1 \pm 0.8$.

of 0.05–0.5,[32] and previous studies have demonstrated that the physics describing the locomotion of *C. elegans* is compatible with that of a low Re swimmer.[32,36] For such low Re swimmers, the forces we measure are dominated by viscous forces.[32] As such, a maximum in the lateral force, for instance, roughly corresponds to the point in the worm's swimming cycle in which it moves with maximal velocity in the negative lateral direction (defined to be right in our experiments). Using the same logic, when the worm has a maximal velocity component in the negative propulsive direction, we measure a maximum force in the forwards swimming direction.

At close distances to the planar boundary, we observe significant increases in the forces generated by the worms. As seen in Figs. 2(a) and 2(b), the lateral and propulsive force curves are plotted as a function of time over one swimming period . Near the boundary, the force curves appear vertically stretched in comparison to the corresponding force curves of the same worm far from the boundary. At large distances from the planar boundary (roughly $h \sim 3000\ \mu$m, or $h/r_w > 100$, where r_w is the radius of the worm), we observe the swimming of the worms to be similar in form and frequency as in previous work in an unbounded fluid.[32] Furthermore, at large distances, the magnitudes of the forces we measure compare well with past work. In Fig. 2(c), the normalized root-mean-square (rms) lateral force is plotted as a function of h/r_w. The rms lateral force increases continuously as the worms are brought closer to the boundary. The rms lateral force increases most significantly below $h/r_w \sim 10$, and at very close approaches to the boundary it can be more than 3 times larger than in an unbounded fluid. For the mean propulsive force, we measure $\langle F_P \rangle = 3 \pm 1$ nN at $h/r_w = 1.8 \pm 0.3$ for worms with $L_{out} = 880 \pm 60\ \mu$m, where L_{out} is the length of the worm found outside of the pipette. In comparison, for worms of similar size in an unbounded fluid, $\langle F_P \rangle = 0.8 \pm 0.2$ nN.[32] Thus, in our experiments, the worms attain significantly larger mean propulsive forces when they swim near the boundary. Near the boundary, viscous drag forces are larger due to the nearby no-slip interface. Since the propulsion of microswimmers is derived from viscous forces, the propulsive forces are expected to increase near the solid boundary because of the increasing velocity gradient.

2. Drag coefficients

For a swimmer moving through a fluid, the velocity of each infinitesimal segment of the swimmer's body can be decomposed into two perpendicular directions, a component tangential (v_T) and normal (v_N) to the body. In RFT, these velocities generate infinitesimal drag forces (dF) on the corresponding body segment (dl), which are given by

$$dF_T = -c_T v_T \mu\, dl \quad \text{and} \quad dF_N = -c_N v_N \mu\, dl, \tag{1}$$

where μ is the dynamic viscosity, c represents the drag coefficient per unit length, and T and N denote directions tangential and normal to the body segment.[25] The ratio c_N/c_T has been estimated through theoretical as well as experimental studies to be approximately 1.5 for *C. elegans* in an infinite fluid medium.[22,26,36] We previously measured these drag coefficients for *C. elegans* in an unbounded fluid to be $c_N = 5.1 \pm 0.3$ and $c_T = 3.4 \pm 0.2$, where the ratio of the drag coefficients, K, was fixed to be 1.5.[32] However, these coefficients have not been experimentally determined in the proximity to a boundary.

If c_N and c_T as well as the speed of each segment of the worm's body are known, one may integrate Eq. (1) to find the total viscous force acting on the undulator. From image analysis of our high speed image sequences attained during experiments, we can extract kinematic data, including body segment speeds, for the worm's swimming. Since c_N and c_T are not known in the presence of a solid boundary, we can treat these as free parameters in calculating RFT's prediction of the lateral and propulsive forces, as each of these forces has contributions from both tangential and normal forces acting on the worm. Using this procedure, we can fit the RFT force curves to the experimental force curves, and as such, extract best fit values for c_N and c_T. A third free parameter is employed in our fits which allows for a relative phase shift between the theoretical and experimental force curves. This horizontal time shift may be present for several reasons, including viscous damping of the micropipette, inertial effects of the worm, and various imaging artifacts. These phase shifts are always smaller than $T/20$, where T is the period of the worm's motion. Examples of RFT fits to

lateral and propulsive force data for a young adult worm swimming near a boundary are shown in Figs. 2(d) and 2(e), where the data are plotted alongside the RFT prediction. As seen in these figures, the RFT fit describes the data within experimental error. In addition, as seen in Figs. 2(d) and 2(e), the experimental force curves are reproducible over time.

The fits are performed at several values of h/r_w for L4, young adult, and adult worms. The swimming of these worms is observed to be approximately self-similar, meaning that the swimming motions and waveforms all scale with the size of the worm. The self-similarity allows these different sized worms to be compared. The resultant values of c_N and c_T are plotted as a function of h/r_w in Figs. 3(a) and 3(b). As demonstrated in these plots, the data collapse for a large range of values of h/r_w, since both h and r_w ($\sim$14 μm to $\sim$35 μm) are varied, this suggests that this ratio is an important controlling parameter.

Katz *et al.* incorporated the effects of a nearby solid planar boundary into the calculation of the drag coefficients for a straight cylinder.[30] Their values of c_N and c_T, which contain no free parameters, are plotted along with the data in Figs. 3(a) and 3(b), represented by the solid curves. In their analysis, the resultant resistance coefficients are derived in the regime $r_0 \ll h \ll l/2$, where r_0 and l are the radius and length of the cylinder, respectively. For a young adult worm in our experiments, $r_w \sim 24$ μm and $L_{out}/2 \sim 450$ μm. The point at which $h/r_w \sim (L_{out}/2)/r_w$ (i.e., $h \sim L_{out}/2$) is indicated by a vertical arrow on the x-axis of Fig. 3(b). Evidently, there is no value of h which is much larger than the worm radius, and simultaneously much smaller than half the worm length. Thus, *C. elegans* falls outside of the ideal regime for which the derivation by Katz *et al.* is applicable.

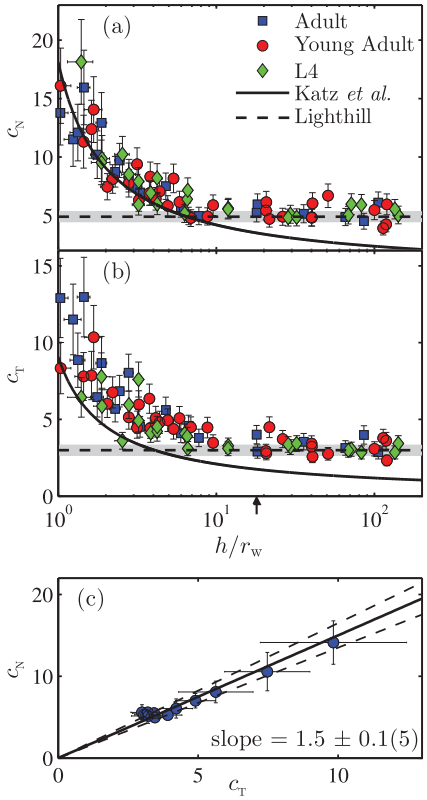

FIG. 3. (a) c_N and (b) c_T plotted against the normalized distance from the boundary for adult, young adult, and L4 worms. The vertical error bars come from uncertainty in the spring constant of the pipette and the fitting procedure. The solid and dashed curves correspond to the predictions of Katz *et al.* and Lighthill.[22,30] The grey area denotes the uncertainty range in evaluating Lighthill's drag coefficients. The vertical arrow on the x-axis of (b) represents the point at which $h \sim L_{out}/2$. (c) Binned values of c_N and c_T from (a) and (b), respectively, demonstrating that a linear fit (solid line) with a slope of $1.5 \pm 0.1(5)$ describes the data within error. The dashed lines correspond to lines given by the upper and lower bounds of the slope. The error bars of the data points come from the scatter in the binning of (a) and (b).

However, there are no studies which incorporate boundary effects into a calculation for the drag coefficients of an undulating cylinder. Thus, although limited in its applicability to our system, the study of Katz *et al.* provides the most relevant comparison near a boundary. Despite this, as seen in Fig. 3(a), their predictions describe the c_N data well for $h/r_w \lesssim 4$. On the other hand, one can see in Fig. 3(b) that there is a consistent underestimate of c_T compared to our measurements for all h/r_w. In the limit $h \gg r_w$, the worm can be well approximated as swimming in an unbounded fluid, where the theoretical predictions of drag coefficients for an undulatory swimmer become applicable.[22,25] In this regime, the wavelength of the swimming is a more relevant length scale than the distance from the boundary, and the prediction of Katz *et al.*, which does not take into account the effects of undulations, is expected to fail. Since Lighthill's resistance coefficients have been shown to exhibit excellent agreement with experimental values in an unbounded fluid,[22,32] we expect the data for c_N and c_T to match this theoretical prediction in the $h \gg r_w$ regime. Indeed, as seen in Figs. 3(a) and 3(b), Lighthill's resistance coefficients, given by $c_N = 4.9 \pm 0.4$, and $c_T = 3.0 \pm 0.3$,[22] represented by dashed lines, agree with the data for $h/r_w \gtrsim 10$. In generating this prediction, we have used parameters characteristic of young adult worms: 1.0 ± 0.2 mm as an estimated wavelength, and $r_w = 45 \pm 5$ μm, but since the swimming can be approximated as self-similar,[32] the theoretical drag coefficients for adults and L4's are within error of the values above.

In Fig. 3(c), binned averaged values of c_N are plotted as a function of binned averaged values of c_T. The binning is performed evenly as a function of $\log_{10}(h/r_w)$ with bin sizes of 0.15, large enough to have sufficient data in each bin. An average value within each bin is subsequently computed. We fit these data to a line constrained to pass through the origin, and obtain a slope of $K = 1.5 \pm 0.1(5)$. Thus, the ratio $K = c_N/c_T$ assumes a constant, distance-independent value of $1.5 \pm 0.1(5)$ for undulatory swimming in a plane parallel to a solid planar boundary. In the straight cylinder calculation of Katz *et al.*, a constant value of $K = 2$ is derived. Lighthill's calculation yields $K = 1.6 \pm 0.2$, which is in agreement with our experimental value for all h/r_w. Interestingly, theoretical and experimental estimates which have suggested that $K \sim 1.5$ have been carried out for an infinite fluid medium,[22,26,36] yet our results imply that this ratio remains valid in the proximity of a solid planar boundary.

As a consistency check, it is worthwhile comparing to see that the increase in the magnitude of the forces we measure close to a boundary, scale with the increase in drag coefficients. Nearby the boundary ($h/r_w = 1.8 \pm 0.3$), where we found $\langle F_P \rangle = 3 \pm 1$ nN, c_N and c_T are both roughly 2.5 times larger than in an unbounded fluid, where $\langle F_P \rangle = 0.8 \pm 0.2$ nN.[32] The mean propulsive force and rms lateral forces should scale linearly with the magnitude of the drag coefficients. Thus, we would expect $\langle F_P \rangle$ near the boundary to be roughly 2.5 times larger than in an unbounded fluid, or $\langle F_P \rangle \sim 2$ nN, which agrees with the measured value within experimental error. Furthermore, the rms lateral force near the boundary is found to be 2.3 ± 0.2 times larger than in an unbounded fluid. This increase is roughly consistent with the 2.5 times increase in the drag coefficients.

B. Channel confinement

For the studies of a worm confined between two solid boundaries (Fig. 1(c)), the confining geometry restricted us to a straight pipette and only lateral forces could be measured. Thus, our resistive force theory curves are, in this case, only fit to lateral force data.[50] In the same way as before, we can extract the values of c_N and c_T from our free fits. The results are shown as a function of h/r_w in Figs. 4(a) and 4(b) for adult, young adult, and L4 worms. For the smallest channel, the drag coefficients are more than an order of magnitude larger compared to in an unbounded fluid. Thus, we see that the effect of a second solid boundary is not simply additive in terms of the increase in the drag coefficients experienced by the worm. Instead, the second boundary imposes a significant restriction on the fluid flow surrounding the worm's body compared to in the single boundary case, causing this large increase in viscous drag.

In their study, Katz *et al.* also investigate the case of parallel plate confinement of a straight cylinder moving in the central plane of the channel.[30] Once again, the derivation is carried out for a straight cylinder in the $r_0 \ll h \ll l/2$ limit, and is thus limited in its applicability to our

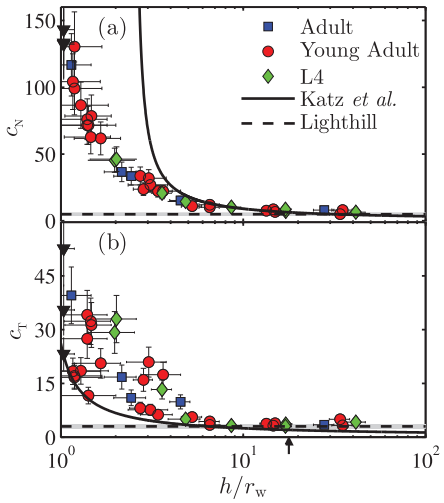

FIG. 4. (a) c_N and (b) c_T as a function of the normalized distance to each boundary in channel confinement for adult, young adult, and L4 worms. The predictions of Katz *et al.* and Lighthill are plotted as solid and dashed curves. The vertical arrow on the x-axis of (b) represents the point at which $h \sim L_{out}/2$. The black triangle markers correspond to three measurements on the same worm at three separate *y*-positions (Fig. 1(c)). This translation affects c_T more significantly than c_N.

system. Nevertheless, for comparison, this theoretical prediction for the drag coefficients, as well as Lighthill's results, are plotted alongside the data in Figs. 4(a) and 4(b). Here we see that the predictions of Katz *et al.* are in agreement with data near the intersection with Lighthill's drag coefficients. For larger h/r_w, Lighthill's results capture our data within error. For smaller h/r_w, the results of Katz *et al.* overestimate c_N and underestimate c_T. The failure is not a failure of the theory, rather it is to be expected since *C. elegans* falls outside of the regime in which the derivation of Katz *et al.* is carried out. Despite this, as mentioned previously, the study of Katz *et al.* provides the most relevant theoretical comparison of drag coefficients near a boundary.

The data of c_T contain more scatter than the data for c_N. We believe that this can in part be attributed to c_T being more influenced by changes in geometry of the experiment. The thin chambers that we use may not be perfectly parallel ($\pm 0.5^\circ$) and the swimming plane of the worm may also be subject to a tilt ($\pm 2^\circ$), such that the swimming of the worm is not exactly in plane with the chamber walls. Furthermore, there is an inherent error in determining the midpoint of the chamber ($\pm 2\ \mu$m). These sources of scatter would be more significant for experiments with higher confinement. To demonstrate the possibility of scatter due to uncertainties in geometry, we performed an experiment in which we placed the worm at the center of a very thin chamber, and measured the drag coefficients at three separate *y*-positions (Fig. 1(c)), each a few hundred micrometers apart. These three measurements are represented by the black triangle markers in Fig. 4. As seen in the figure, this procedure resulted in significant scatter in the value of c_T, yet relatively little scatter in the value of c_N, where two of the data points are so close that they are indistinguishable in the plot. Another source of scatter may stem from the RFT fitting. Since the final contribution of tangential body motion to the lateral force is smaller than the contribution from normal body motion, our fits will be more sensitive to determining c_N precisely.

Interestingly, the predictions of Katz *et al.* involve a monotonically increasing value of K upon increasing the confinement within the channel, in contrast with the case of the single boundary. In our experiments, we find that for very large channels (at $h/r_w = 35 \pm 6$), $K = 1.8 \pm 0.7$, which is in agreement with the results for an essentially unbounded fluid (i.e., far from the single plane boundary). On the other hand, for very narrow channels (at $h/r_w = 1.3 \pm 0.1$), we find $K = 5 \pm 2$. Thus, when confined between two plates there is an increase in K for highly confined worms, whereas we obtain a constant value of K for an undulatory swimmer near a single plane boundary.

C. Gait modulation

For very wide channels, or at large distances from a single boundary, the same swimming is seen as for an unbounded fluid.[32] However, as the worm is placed into channels of high confinement, there is a significant difference in the swimming of the worm (see movies in the supplementary material (Multimedia view)[50]). Most noticeably, the amplitude of the motion is greatly reduced compared to that seen in an unbounded fluid. Time-lapses of the nematode's centerline over one period of motion are shown in Figs. 5(a) and 5(b), for $h/r_w = 28 \pm 4$ and $h/r_w = 1.1 \pm 0.3$. For the highly confined worm, the shape of the worm's body is more akin to a sinusoid about the swimming axis, and more similar to the free swimming waveform of *C. elegans*.[35,36] In Fig. 5(c), the lateral position of the head of the worm (x_{head}) is plotted as a function of time for the worm in low and high channel confinements, corresponding to Figs. 5(a) and 5(b). As seen, the amplitude of the worm's head motion is much larger when it is not confined (red open circle markers) compared to under high confinement (blue filled circle markers). In addition, the confined worm is seen to swim with a reduced frequency.

To quantify the change of amplitude discussed above, experienced by the worm as it modulates its gait, we measure the mean angular amplitude, A_θ, which is defined as half the angle swept out by the worm's head during swimming. As seen in Figs. 5(a) and 5(b), the angular amplitude is significantly smaller for the confined worm. Since it is known that *C. elegans* experiences a gait modulation in response to increasing environmental resistance (such as increasing viscosity), it is not surprising that the swimming form will change with increasing values of c_N and c_T. In our system, we quantify the amount of environmental resistance by the sum $c_N + c_T$, which increases by a factor of 20 from an unbounded fluid to the most confined worms studied (analogous to a 20-fold increase in viscosity from that of a buffer, as seen in Eq. (1)). The angular amplitude is plotted as a function of $c_N + c_T$ in Fig. 5(d) for worms swimming in channel confinement as well as in the presence

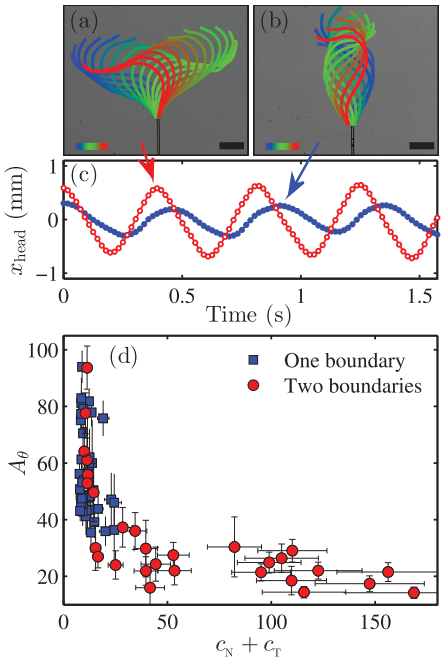

FIG. 5. Time-lapses of the worm's centerline over one swimming period for (a) very low ($h/r_w = 28 \pm 4$) and (b) very high ($h/r_w = 1.1 \pm 0.3$) confinement, in which only every other centerline in the image sequence is plotted. The colourbar indicates the temporal progression along the single period (from t = 0 to t = T) and the scalebar represents 200 μm. (c) The lateral position of the head (x_{head}) of the worm in high and low channel confinement as a function of time for several swimming periods. The red open circles and the blue filled circles correspond to the worms in (a) and (b). (d) The angular amplitude as a function of $c_N + c_T$ for young adult and adult worms swimming near a single boundary (blue squares) and in channel confinement (red circles).

of a single boundary. The angular amplitude decreases as a function of $c_N + c_T$. This decrease is most rapid for $c_N + c_T \lesssim 30$. In addition, since the worm simply modulates its gait in response to changing resistance, the results for the single boundary and for the channel confinement fall on the same curve. Included in this gait modulation is a slight decrease in the swimming frequency from 2.4 ± 0.2 Hz for an unbounded fluid,[32] to 2.07 ± 0.13 Hz for $c_N + c_T = 108 \pm 9$.

The significant difference in swimming amplitude that we measure by confining the worm has not been seen over the same range of increasing environmental resistance in studies of gait modulation in which the fluid viscosity has been changed.[35,36] In these studies, the amplitude of free swimming worms was found to remain relatively constant over a 20-fold increase in the viscosity from that of a buffer. However, the fact that our worm is tethered at the tail is a crucial difference, and the swimming amplitude we measure in the unbounded buffer differs from that of a free swimming worm. Therefore, it is not surprising that some kinematic parameters, such as the amplitude, may exhibit different behaviours in the gait modulation of our system. Studies on gait modulation in *C. elegans* measure a decrease in the swimming frequency of roughly 10%–20% from that in a buffer,[35,36] which is consistent with our findings. In studying gait modulation by changing the viscosity, the chemical composition of the fluid is altered, which may have implications on the behaviour of the worm. In addition, the osmotic pressure of the solution is changed, which may upset the ionic balance of the nematode. Therefore, our results indicate that confinement near solid boundaries is another complimentary way in which gait modulation can be investigated without changing composition of the fluid.

IV. SUMMARY AND CONCLUSIONS

In this study, we present an experimental investigation into drag forces acting on an undulatory microswimmer in proximity to solid boundaries. We employ micropipette deflection to directly measure the viscous forces during the swimming of the model organism *C. elegans* in a plane parallel to nearby boundaries. This represents the first direct force measurement of a microswimmer in which boundary effects have been investigated. We witness large increases in the lateral and propulsive forces of the worm as it approaches a single boundary. Using kinematic data from the high speed image sequences of the swimming in conjunction with our force measurements, we are able to extract the normal and tangential drag coefficients for the worm. The drag coefficients decrease as a function of the distance away from the solid boundary. Despite the study being limited in its applicability to our experimental system, the predictions of Katz *et al.* capture the general trends of c_N and c_T near the boundary, but with some deviations. Lighthill's results for c_N and c_T are successful at large separations from the boundary. We find $K = c_N/c_T = 1.5 \pm 0.1(5)$ at *all* distances from the boundary. This is an interesting result, as it suggests that a propulsive force increase of an undulator swimming in plane with a nearby boundary cannot be attributed to a changing ratio of the drag coefficients.

For confinement between two planar boundaries, the drag coefficients increase by a factor of 20 for the highest confinements compared to in an unbounded fluid, and we observe an increase in K for high confinements. In this geometry, Lighthill's results are still in agreement with our data for very large channels. Our results suggest that the analytical results for the drag coefficients in proximity to a boundary are not entirely suitable for this system, and require reconsideration by further theoretical studies. For both channel and single boundary geometries, as the drag coefficients increase, the nematode is seen to undergo a gait modulation characterized by a large decrease in the amplitude of its swimming. This gait modulation is independent of whether the worm is swimming near one or two boundaries, and is only a function of the drag coefficients it is experiencing. These results offer a promising new means of investigating the gait modulation of *C. elegans* by confining the worm, rather than changing the viscosity and hence altering the chemical composition of the fluid.

ACKNOWLEDGMENTS

The financial support by Natural Science and Engineering Research Council of Canada is gratefully acknowledged. The authors also thank Alexandra Kasper for useful comments.

[1] E. M. Purcell, "Life at low Reynolds-number," Am. J. Phys. **45**, 3–11 (1977).
[2] R. P. McCord, J. N. Yukich, and K. K. Bernd, "Analysis of force generation during flagellar assembly through optical trapping of free-swimming *Chlamydomonas reinhardtii*," Cell Motil. Cytoskel. **61**, 137–144 (2005).
[3] S. Chattopadhyay, R. Moldovan, C. Yeung, and X. L. Wu, "Swimming efficiency of bacterium *Escherichia coli*," Proc. Natl. Acad. Sci. U.S.A. **103**, 13712–13717 (2006).
[4] Y. W. Kim and R. R. Netz, "Pumping fluids with periodically beating grafted elastic filaments," Phys. Rev. Lett. **96**, 158101 (2006).
[5] M. J. Kim and K. S. Breuer, "Microfluidic pump powered by self-organizing bacteria," Small **4**, 111–118 (2008).
[6] E. Lauga and T. R. Powers, "The hydrodynamics of swimming microorganisms," Rep. Prog. Phys. **72**, 096601 (2009).
[7] M. J. Kim and K. S. Breuer, "Enhanced diffusion due to motile bacteria," Phys. Fluids **16**, L78–L81 (2004).
[8] M. J. Kim and K. S. Breuer, "Controlled mixing in microfluidic systems using bacterial chemotaxis," Anal. Chem. **79**, 955–959 (2007).
[9] N. Darnton, L. Turner, K. Breuer, and H. C. Berg, "Moving fluid with bacterial carpets," Biophys. J. **86**, 1863–1870 (2004).
[10] D. B. Weibel, P. Garstecki, D. Ryan, W. R. Diluzio, M. Mayer, J. E. Seto, and G. M. Whitesides, "Microoxen: Microorganisms to move microscale loads," Proc. Natl. Acad. Sci. U.S.A. **102**, 11963–11967 (2005).
[11] G. L. Cooper, A. L. Schiller, and C. C. Hopkins, "Possible role of capillary action in pathogenesis of experimental catheter-associated dermal tunnel infections," J. Clin. Microbiol. **26**, 8–12 (1988).
[12] G. Harkes, J. Dankert, and J. Feijen, "Bacterial migration along solid surfaces," Appl. Environ. Microbiol. **58**, 1500–1505 (1992).
[13] S. S. Suarez and A. A. Pacey, "Sperm transport in the female reproductive tract," Hum. Reprod. Update **12**, 23–37 (2006).
[14] J. W. Costerton, Z. Lewandowski, D. E. Caldwell, D. R. Korber, and H. M. Lappin-Scott, "Microbial biofilms," Annu. Rev. Microbiol. **49**, 711–745 (1995).
[15] M. C. Van Loosdrecht, J. Lyklema, W. Norde, and A. J. Zehnder, "Influence of interfaces on microbial activity," Microbiol. Rev. **54**, 75–87 (1990).
[16] D. F. Katz, T. D. Bloom, and R. H. Bondurant, "Movement of bull spermatozoa in cervical mucus," Biol. Reprod. **25**, 931–937 (1981).
[17] E. Lauga, W. R. DiLuzio, G. M. Whitesides, and H. A. Stone, "Swimming in circles: Motion of bacteria near solid boundaries," Biophys. J. **90**, 400–412 (2006).
[18] W. R. DiLuzio, L. Turner, M. Mayer, P. Garstecki, D. B. Weibel, H. C. Berg, and G. M. Whitesides, "*Escherichia coli* swim on the right-hand side," Nature (London) **435**, 1271–1274 (2005).
[19] U. Ruffer and W. Nultsch, "High-speed cinematographic analysis of the movement of *Chlamydomonas*," Cell Motil. **5**, 251–263 (1985).
[20] M. Polin, I. Tuval, K. Drescher, J. P. Gollub, and R. E. Goldstein, "*Chlamydomonas* swims with two "gears" in a eukaryotic version of run-and-tumble locomotion," Science **325**, 487–490 (2009).
[21] M. Silverman and M. Simon, "Flagellar rotation and the mechanism of bacterial motility," Nature (London) **249**, 73–74 (1974).
[22] J. Lighthill, "Flagellar hydrodynamics – The John von Neumann Lecture, 1975," SIAM Rev. **18**, 161–230 (1976).
[23] G. Taylor, "Analysis of the swimming of microscopic organisms," Proc. R. Soc. London A **209**, 447–461 (1951).
[24] J. Gray, "Undulatory propulsion," Q. J. Microsc. Sci. **94**, 551–578 (1953).
[25] J. Gray and G. J. Hancock, "The propulsion of sea-urchin spermatozoa," J. Exp. Biol. **32**, 802–814 (1955).
[26] J. Gray and H. W. Lissmann, "The locomotion of nematodes," J. Exp. Biol. **41**, 135–154 (1964).
[27] G. Tokic and D. K. P. Yue, "Optimal shape and motion of undulatory swimming organisms," Proc. R. Soc. B **279**, 3065–3074 (2012).
[28] R. G. Cox, "The motion of long slender bodies in a viscous fluid. Part 1. General theory," J. Fluid Mech. **44**, 791–810 (1970).
[29] R. S. Berman, O. Kenneth, J. Sznitman, and A. M. Leshansky, "Undulatory locomotion of finite filaments: Lessons from *Caenorhabditis elegans*," New J. Phys. **15**, 075022 (2013).
[30] D. F. Katz, J. R. Blake, and S. L. Paveri-Fontana, "On the movement of slender bodies near plane boundaries at low Reynolds number," J. Fluid Mech. **72**, 529–540 (1975).
[31] N. J. De Mestre, "Low-Reynolds-number fall of slender cylinders near boundaries," J. Fluid Mech. **58**, 641–656 (1973).
[32] R. D. Schulman, M. Backholm, W. S. Ryu, and K. Dalnoki-Veress, "Dynamic force patterns of an undulatory microswimmer," Phys. Rev. E **89**, 050701 (2014).
[33] S. Brenner, "The genetics of *Caenorhabditis elegans*," Genetics **77**, 71–94 (1974).
[34] M. Backholm, W. S. Ryu, and K. Dalnoki-Veress, "Viscoelastic properties of the nematode *Caenorhabditis elegans*, a self-similar, shear-thinning worm," Proc. Natl. Acad. Sci. U.S.A. **110**, 4528–4533 (2013).
[35] C. Fang-Yen, M. Wyart, J. Xie, R. Kawai, T. Kodger, S. Chen, Q. Wen, and A. D. T. Samuel, "Biomechanical analysis of gait adaptation in the nematode *Caenorhabditis elegans*," Proc. Natl. Acad. Sci. U.S.A. **107**, 20323–20328 (2010).
[36] J. Sznitman, X. Shen, R. Sznitman, and P. E. Arratia, "Propulsive force measurements and flow behavior of undulatory swimmers at low Reynolds number," Phys. Fluids **22**, 121901 (2010).
[37] X. N. Shen, J. Sznitman, P. Krajacic, T. Lamitina, and P. E. Arratia, "Undulatory locomotion of *Caenorhabditis elegans* on wet surfaces," Biophys. J. **102**, 2772–2781 (2012).
[38] X. N. Shen and P. E. Arratia, "Undulatory swimming in viscoelastic fluids," Phys. Rev. Lett. **106**, 208101 (2011).
[39] P. Sauvage, M. Argentina, J. Drappier, T. Senden, J. Siméon, and J.-M. Di Meglio, "An elasto-hydrodynamical model of friction for the locomotion of *Caenorhabditis elegans*," J. Biomech. **44**, 1117–1122 (2011).
[40] S. Park, H. Hwang, S.-W. Nam, F. Martinez, R. H. Austin, and W. S. Ryu, "Enhanced *Caenorhabditis elegans* locomotion in a structured microfluidic environment," PLoS One **3**, e2550 (2008).
[41] T. Majmudar, E. E. Keaveny, J. Zhang, and M. J. Shelley, "Experiments and theory of undulatory locomotion in a simple structured medium," J. R. Soc. Interface **9**, 1809–1823 (2012).

[42] G. Juarez, K. Lu, J. Sznitman, and P. E. Arratia, "Motility of small nematodes in wet granular media," Europhys. Lett. **92**, 44002 (2010).
[43] S. Jung, "*Caenorhabditis elegans* swimming in a saturated particulate system," Phys. Fluids **22**, 031903 (2010).
[44] F. Lebois, P. Sauvage, C. Py, O. Cardoso, B. Ladoux, P. Hersen, and J.-M. Di Meglio, "Locomotion control of *Caenorhabditis elegans* through confinement," Biophys. J. **102**, 2791–2798 (2012).
[45] A. Ghanbari, V. Nock, S. Johari, R. Blaikie, X. Chen, and W. Wang, "A micropillar-based on-chip system for continuous force measurement of *C. elegans*," J. Micromech. Microeng. **22**, 095009 (2012).
[46] J. C. Doll, N. Harjee, N. Klejwa, R. Kwon, S. M. Coulthard, B. Petzold, M. B. Goodman, and B. L. Pruitt, "SU-8 force sensing pillar arrays for biological measurements," Lab Chip **9**, 1449–1454 (2009).
[47] R. Ghosh and J. Sznitman, "Visualization of nematode *Caenorhabditis elegans* swimming in a liquid drop," J. Vis. **15**, 277–279 (2012).
[48] M.-J. Colbert, A. N. Ragen, C. Fradin, and K. Dalnoki-Veress, "Adhesion and membrane tension of single vesicles and living cells using a micropipette-based technique," Eur. Phys. J. E **30**, 117–121 (2009).
[49] M.-J. Colbert, F. Brochard-Wyart, C. Fradin, and K. Dalnoki-Veress, "Squeezing and detachment of living cells," Biophys. J. **99**, 3555–3562 (2010).
[50] See supplementary material at http://dx.doi.org/10.1063/1.4897651 for examples of RFT fits for swimming near one and two boundaries, and for movies of the worm swimming before and after confinement.